Published in final edited form as:
J Cereb Blood Flow Metab. 2008 April ; 28(4): 674–683. doi:10.1038/sj.jcbfm.9600587.

Changes in autophagy after traumatic brain injury

Cindy L Liu[1], **Shaoyi Chen**[1], **Dalton Dietrich**[2], and **Bingren R Hu**[1]

1*Neurochemistry Laboratory of Brain Injury, Department of Neurology, University of Miami School of Medicine, Miami, Florida, USA*

2*Department of Neurosurgery and the Miami Project to Cure Paralysis, University of Miami School of Medicine, Miami, Florida, USA*

Abstract

Autophagy is the chief machinery for bulk degradation of superfluous or aberrant cytoplasmic components. This study used the rat moderate fluid percussion injury model to investigate whether the autophagy pathway plays a key role after traumatic brain injury (TBI). Induction of autophagy is manifested by accumulation of autophagosomes (APs), observable under transmission electron microscopy (EM). Two hallmarks of autophagy, i.e., the microtubule-associated protein light chain 3 (LC3)-II and the autophagy-related gene (ATG)12-ATG5 conjugates, were explored by biochemical and confocal microscopic analyses of brain tissues. Under EM, both APs and autolysosomes were markedly accumulated in neurons from 4 h onward after TBI. Western blot analysis showed that ATG12-ATG5 conjugate was markedly redistributed during 5 to 15 days in brain tissues after TBI. LC3-II conjugate was initially unchanged but was drastically upregulated from 24 h onward in the pre-AP-containing fraction after TBI. LC-3 immunostaining was mainly located in living neurons under confocal microscopy. These results clearly show that the autophagy pathway is persistently activated after TBI. Because the autophagy pathway is the chief machinery for bulk elimination of aberrant cell components, we propose that activation of this pathway serves as a protective mechanism for maintaining cellular homeostasis after TBI.

Keywords

ATG12-ATG5; autophagy; LC3-ATG8-APG8; lysosome; traumatic brain injury; ubiquitin

Introduction

There are two major known routes for clearance of aberrant components in eukaryotic cells: (i) the ubiquitin–proteasomal pathway and (ii) the autophagy –lysosomal pathway. The ubiquitin–proteasomal pathway is responsible for degradation of short-lived proteins and has been studied intensively during the past decades, including in brain injury (Hu *et al*, 2000; Hu, 2006; Ciechanover, 2006). The autophagy pathway, originally described as a stress response to nutrient deprivation, is now emerging as the chief route for bulk degradation of *aberrant* organelles, protein aggregates, and invading foreign materials (Nixon, 2006). There are three basic types of autophagy: macroautophagy, microautophagy, and chaperone-mediated autophagy. Bulk degradation of cytoplasmic organelles is largely mediated by macroautophagy, which is commonly referred to as autophagy (hereafter). Autophagy is a nonstop lifesustaining renewal process that is active under normal conditions and is further enhanced in response to tissue injury (Klionsky, 2005).

Correspondence: Dr BR Hu, Department of Neurology, University of Miami School of Medicine, PO Box 16960, Miami, Florida 33136, USA. E-mail: E-mail: cliu@med.Miami.edu.

The molecular mechanisms underlying autophagy have just begun to emerge: (i) a group of autophagy-related genes (*atgs*) and their encoded proteins (ATGs) have been identified by genetic screens in yeast and fungi; and (ii) human homologues of the highly conserved ATGs have been discovered and tied to specific human genetic diseases (Kiselyov *et al*, 2007). Autophagy starts with the formation of double-membraned cisternae that subsequently engulf cytoplasmic materials or whole organelles to become double-membrane bubblelike vacuoles known as autophagosomes (APs). After maturation, APs merge with lysosomes for bulk degradation of the cargo contents (Yorimitsu and Klionsky, 2005). Hence, the appearance of APs under transmission electron microscopy (EM) is a morphologic hallmark unique to autophagy. Two biochemical markers, also unique to autophagy, are the covalent conjugates of (i) ATG12-ATG5 and (ii) microtubule-associated protein light chain 3 (LC3)-phosphatidylethanolamine (PE). Microtubule-associated protein light chain 3 is a mammalian homologue of yeast ATG8 and it is synthesized as a pro-LC3. After synthesis, pro-LC3 is cleaved by ATG4 protease and becomes the 16 to 18 kDa LC3-I. On activation of autophagy, LC3-I is conjugated with PE (lipidated). The lipidated form is referred to as LC3-II (Kabeya *et al*, 2004). The conjugation to create ATG12-ATG5 or LC3-II is performed by two consecutive ubiquitinationlike enzyme systems in an ATP-dependent manner, involving ATG7 and ATG10 for ATG12-ATG5 conjugation, and ATG7 and ATG3 for LC3-II conjugation (Klionsky, 2005). After conjugation, both ATG12-ATG5 and LC3-II become structural components of the double-membraned cisterns or APs and are thus redistributed among the membrane fractions. Therefore, the protein levels and redistribution of ATG5-ATG12 and/or LC3-II conjugates in the membrane fractions are often used as a measure to determine autophagic activity (Kabeya *et al*, 2004).

Traumatic brain injury (TBI) is a serious and debilitating health problem affecting millions of people each year (http://www.ninds.nih.gov). Traumatic brain injury leads to brain tissue damage and cognitive impairment (Bramlett and Dietrich, 2004). Although remarkable progress has been made in pathophysiology, molecular events after TBI are still incompletely understood. This study used the rat fluid percussion injury model to investigate whether the autophagy pathway is involved in TBI tissue damage and repair. The results clearly show that autophagy is induced significantly after TBI. Induction of autophagy after TBI may be responsible for eliminating aberrant cellular components, thus maintaining cellular homeostasis after TBI.

Materials and methods

Traumatic Brain Injury Model

Experiments were performed with male Sprague–Dawley rats weighing 270 to 320 g (Charles River Laboratories, Raleigh, NC, USA). All experimental procedures were in compliance with the NIH *Guide for the Care and Use of Laboratory Animals* and approved by the University of Miami Animal Care and Use Committee. All feasible measures were taken to reduce animal suffering and the numbers of animals used for these experiments. The basic surgical preparation for brain injury was performed according to previously described methods (Dietrich *et al*, 1996). Briefly, animals were maintained for at least 7 days before the experiment in a temperature-regulated room (23°C to 25°C) on a 12-h light/dark cycle. The rats were fasted but allowed free access to water overnight before surgery. Moderate TBI was produced with fluid percussion pressure levels of 2.0±0.2 atmosphere (atm). Rats were anesthetized with 3.0% halothane in a gas mixture of 70% N_2O and 30% O_2. The femoral artery was cannulated to deliver pancuronium bromide (0.5 mg/kg, intravenously) every 1 h during the surgical procedure to immobilize the rats. An endotracheal tube was inserted, and the rats were mechanically ventilated with 70% N_2O, 0.5% to 1.5% halothane, and a balance of O_2. The animals were then placed in a stereotaxic frame and a 4.8mm craniotomy was made over the

right parietal cortex (3.8mm posterior to bregma, 2.5mm lateral to the midline). A plastic injury tube (18 gauge modified Precision-Glide needle hub; Becton Dickinson, Franklin Lakes, NJ, USA) was placed over the exposed dura and fixed with dental acrylic. Before and after TBI, blood gases and mean arterial blood pressure were monitored and maintained at physiologic levels. Brain temperature was monitored with a thermistor probe placed in the left temporalis muscle, whereas core temperature was determined with a rectal thermometer. Brain temperature was maintained at 37°C with self-adjusting feedback heating lamps. Blood gases, blood glucose, and hematocrit values were monitored 15 mins before TBI, 15 mins after TBI, and then once every hour for up to 4 h after TBI. All animals were maintained within physiologic ranges for mean arterial pressure (120 to 140mmHg), pO_2 blood gas levels (105 to 170mmHg), pCO_2 blood gas levels (35 to 45mmHg), and blood pH (7.38 to 7.41).

Six experimental groups, each group consisting of four rats, were used for the biochemical, confocal microscopic, and EM studies. Sham-operated rats were subjected to identical surgical procedures but without the fluid percussion injury pulse. After TBI, anesthesia was discontinued and the animals were returned to their cages. At 4 h, and 1, 3, 5, and 15 days after TBI, the animals were anesthetized, tracheotomized, and artificially ventilated with 70% N_2O, 0.5% to 1.5% halothane, and a balance of O_2. The animals' respiration was maintained with the ventilator while the brains were frozen *in situ* with liquid nitrogen. Afterward, the brains were carefully removed from the liquid nitrogen-frozen heads with a saw, a hammer, and a chisel. The right, injured ipsilateral parietal cortex was dissected in a glove box freezer (−12°C) as described previously (Hu *et al*, 1998). This brain dissection method prevents brain biochemical changes during the processes of decapitation and isolation of brains from the skull (Ponten *et al*, 1973). For EM and confocal microscopy, animals were anesthetized and ventilated with a respirator. They were then perfused with ice-cold 2% glutaraldehyde and 2.5% paraformaldehyde in 0.1mmol/L cacodylate buffer (pH 7.4) for EM, and in 4% paraformaldehyde made with phosphate-buffered saline for confocal microscopy. Brains were post-fixed in the same fixatives for 24h and then sectioned with a vibratome (100 μm for EM; 50μm for confocal microscopy) (Leica Microsystems Inc., Exton, PA, USA).

Transmission Electron Microscopy

Electron microscopy was conducted with brain sections from sham-operated control rats and rats subjected to TBI followed by 4 h, and 1, 3, 5, and 15 days of recovery. Brain tissues were stained by the conventional osmium–uranyl–lead method, as described previously (Martone *et al*, 1999; Liu *et al*, 2005). Briefly, coronal brain sections (100 μm) were cut with a vibratome, postfixed with 4% glutaraldehyde in 0.1 mmol/L cacodylate buffer (pH 7.4) for 1 h, and then with 1% osmium tetroxide in 0.1 mmol/L cacodylate buffer for 2 h. After rinsing with distilled water, the brain sections were treated with 1% aqueous uranyl acetate overnight, dehydrated in an ascending series of ethanols to 100%, followed by dry acetone, and then embedded in Durcupan ACM. Ultrathin sections (0.1 μm) were cut and stained with 3% lead citrate and subsequently examined with a Zeiss transmission electron microscope (Zeiss Inc., Thornwood, NY, USA).

Confocal Microscopy

Fluorescence confocal microscopy was performed on coronal brain sections (50 μm) in the cortical injury region according to the method of Hu *et al* (2000). Brain sections were obtained from sham-operated control rats and from rats subjected to 2.0 atm TBI followed by 24 h of recovery. At least four different sections prepared from four sham surgery animals and four TBI surgery animals, respectively, were used. Sections were washed in Tris-buffered saline (TBS) and then in 0.01 mol/L sodium citrate buffer pH 6.0 for 5 mins. For antigen retrieval, sections were heated for 10 mins at 100°C. Nonspecific binding was blocked with 3% bovine serum albumin in TBS and 0.1% Triton X-100 for 60 mins. Sections were incubated overnight

at 4°C with LC-3 (1:1,000; Cell Signaling Technology, Beverly, MA, USA) antibody diluted in TBS, 0.1% Triton X-100, and 1% bovine serum albumin. After washing with TBS, the sections were incubated with fluorescein-labeled anti-rabbit secondary antibody (1:200; Molecular Probes, Carlsbad, CA, USA) in TBS and 1% bovine serum albumin for 1 h at room temperature. Sections were washed in TBS, mounted with Vectashield mounting medium (Vector Laboratories Inc., Burlingame, CA, USA), and analyzed on a laser-scanning confocal microscope (Zeiss Inc.).

Preparation of Subcellular Fractions

To assess autophagic protein subcellular redistribution after TBI, subcellular fractions were prepared from sham-operated rats and rats subjected to moderate (2.0 atm) TBI followed by 4 h, and 1, 3, 6, and 15 days of recovery. Traumatic brain-injured vulnerable neocortical tissues were dissected and chopped into small pieces in a −15°C glove box freezer, and then homogenized on ice with a Dounce homogenizer (35 strokes, 4°C) in 10 volumes of homogenization buffer containing 15 mmol/L Tris, pH 7.6, 0.25mol/L sucrose, 1mmol/LMgCl$_2$, 2.5mmol/L EDTA, 1 mmol/L EGTA (ethylene glycol-bis (β-amino ethyl ether) tetraacetic acid), 1 mmol/L dithiothreitol, 1.25 μg/mL pepstatin A, 10 μg/mL leupeptin, 2.5 μg/mL aprotinin, 0.5 mmol/L phenylmethylsulfonyl fluoride, 0.1 mmol/L Na_3VO_4, 50 mmol/L NaF, and 2 mmol/L $Na_4P_2O_7$. Homogenates were centrifuged at 800*g* at 4°C for 10 mins to obtain P1 pellets (containing the heaviest cellular components, including the nuclei and secondary lysosomes) and supernatants (S1). The S1 was further centrifuged at 10,000*g* at 4°C for 10 mins to obtain crude cell membrane/synaptosomal/mitochondrial pellet (P2) and its supernatant (S2). The S2 were centrifuged again at 165,000*g* at 4°C for 1 h to obtain the cytosol S3 and the microsomal pellet P3 that contains intracellular membrane structures such as the endoplasmic reticulum and Golgi. All pellet fractions were suspended in homogenization buffer containing 0.1% Triton X-100. Each subcellular fraction was assayed for total protein concentration using the Coomassie Plus assay kit (Bio-Rad Laboratories, Hercules, CA, USA).

Western Blot Analysis

Equal protein amounts in subcellular fractions were electrophoresed on 12.5% (for LC3-II) and 10% (for the rest of the autophagy-related proteins) sodium dodecyl sulfate-polyacrylamide gels and then transferred to Immobilon-P membranes (Millipore, Billerica, MA, USA). The membranes were blocked with 3% bovine serum albumin in TBS for 30 mins and then incubated overnight at 4°C with the following primary ATG antibodies: ATG5 (1:5,000; Cell Signaling Technology) and LC3 (1:3,000, Abgent, San Diego, CA, USA, catalog no. AP1802a; or 1:10,000; Cell Signaling Technology). The membranes were then incubated with horseradish peroxidase-conjugated anti-rabbit or anti-mouse secondary antibodies for 60 to 120 mins at room temperature (1:1,000; Cell Signaling Technology). In addition to the loading of the same protein amounts in subcellular fractions on sodium dodecyl sulfate-polyacrylamide gels, β-actin levels were determined by immunoblotting (1:2,000; Cell Signaling Technology) and were used as endogenous controls for protein loads on the gels. The blots were developed using enhanced chemiluminescence (Amersham Biosciences, Piscataway, NJ, USA) and developed on Kodak X-omat LS film (Eastman Kodak Company, New Haven, CT, USA). Densitometry was performed with Kodak ID image analyses software (Eastman Kodak Company).

Statistical Analysis

Data are expressed as mean±s.d. (n=4) and as a percentage of sham-operated control levels. One-way analyses of variance followed by Dunnett's tests were used for statistical analysis. *$P < 0.05$ between sham and TBI animals.

Results

Ultrastructural Features of Autophagic Maturation after Traumatic Brain Injury

To determine whether autophagic activity is altered after TBI, we first examined brain sections by transmission EM. The EM manifestation of bubble-like vacuoles that enclose recognizable cytoplasmic structures still represents the gold standard for identifying APs (Brunk and Terman, 2002). Preexisting APs were occasionally seen in sham-operated control cortical neurons (Figure 1A). Neurons subjected to TBI followed by recovery, however, displayed a striking increase in the density of APs (Figures 1B to 1F). Neocortical neurons from sham-operated control rats contained polyribosomes (arrows), nucleus (N), rough endoplasmic reticulum (ER), and mitochondria (M) (Figure 1A). At 4 h post-TBI (Figure 1B), the dominant ultrastructural changes were (i) mild accumulation of APs and autolysosomes (ALs) and (ii) mild mitochondrial swelling (M). During 24 h to 15 days post-TBI (Figures 1C to 1F), APs and ALs accumulated markedly, whereas polyribosomes (arrows), mitochondria (M), the endoplasmic reticulum (ER) and Golgi apparatus (G) appeared normal in TBI neurons.

Several morphologic features of AP maturation were clearly observed in neurons at different periods of recovery after TBI (Figure 2). Autophagosome formation began with isolation membranes, i.e., the formation of double-membraned cisterns in the cytoplasm after TBI (Figure 2A, arrows). The double-membraned cisterns enveloped cytoplasmic contents or whole organelles to form APs (Figure 2A, AP). The formation of double membranes and APs was seen as early as 4 h after TBI (Figure 2A) and was an ongoing process during the post-TBI phase (see biochemical analysis below). Autophagosome clusters containing membrane whorls, probably representing damaged mitochondria (M), were frequently seen in dendritic trunks (Figure 2C) and neuronal process-rich regions (neuropil) (Figure 2B) after TBI. Autophagosomes eventually merged with lysosomes to become ALs (Figure 2D). Partially degraded cargo contents within ALs were then manifested as unevenly distributed dense (dark) masses (Figure 2D, AL) and eventually as evenly distributed dense (dark) materials (Figure 2A, AL).

ATG12-ATG5 and LC3-II Conjugation after Traumatic Brain Injury

The biochemical hallmark of autophagic initiation is the consecutive formation of two key ATG conjugates: first ATG12-ATG5, followed by LC3-II (LC3-II is a mammalian homologue of yeast ATG8-PE). After conjugation, ATG12-ATG5 and LC3-II became components of double-membraned cisterns and/or AP and hence were distributed into membrane fractions. We therefore prepared brain tissue homogenate (H) as well as standard P1, P2, P3, and S3 subcellular fractions from neocortical brain tissues subjected either to sham surgery or TBI followed by 4 h, and 1, 3, 5, and 15 days of recovery. To ensure equal loading of protein samples on immunoblots, β-actin immunoreactivity was measured by Western blotting and used as an endogenous control. As shown in Figure 3A, β-actin immunoreactivity on immunoblots was not significantly altered in brain tissue homogenate and any subcellular fraction after TBI. ATG5 antibody was primarily labeled the ATG12-ATG5 conjugated form (~53 kDa) in all subcellular fractions (Figure 3B), whereas the unconjugated (free form) ATG5 (~32 kDa) was barely detected in the homogenate (H) and S3 fraction (Figure 3B, H and S3, arrowhead). Relative to sham-operated controls, the ATG12-ATG5 conjugate was not significantly changed in tissue homogenate (H) and P1 fraction, but was significantly upregulated in the P2 fraction at 3 days of reperfusion after TBI (Figures 3B and 3C). In comparison with P1 and P2 fractions, ATG12-ATG5 in the pre-AP-containing P3 fraction was drastically downregulated at 4 h of recovery and then rebounded significantly above the control level during 5 to 15 days of recovery after TBI (Figures 3B and 3C). ATG12-ATG5 in S3 fraction tended to decrease, but the difference did not reach statistical significance during 1 to 15 days of recovery after TBI

(Figures 3B and 3C). In addition, the ATG12-ATG5 level was the highest in S3 fraction, followed by P3 fraction, and much lower in P1 and P2 fractions (Figure 3B).

Microtubule-associated protein light chain 3 is synthesized as a proform that is cleaved by ATG4 protease to become LC3-I (Tanida *et al*, 2004). Microtubule-associated protein light chain 3-I conjugates covalently with a neutral lipid PE via its C-terminal glycine residue to form lipidated LC3-II, which has a faster mobility on immunoblots. Thus, the N-terminal LC3 antibody was able to recognize both the upper LC3-I band and the lower LC3-II band in homogenate (H) as well as in P1, P2, and P3 fractions, and also pro-LC3 and LC3-I in the cytosolic (S3) fraction (Figure 4A), consistent with previous studies (Tanida *et al*, 2004). After conjugation, LC3-II became a component of the AP and then the AL membranes and hence was distributed mainly to P1 and P2 fractions and to a much lesser degree also to P3 fraction after TBI (Figure 4A). The LC3-I level tended to decrease in H, P1, P2, and P3 fractions, although the changes did not reach statistical significance, probably owing to its large residual contents in these fractions (Figure 4A, LC3-I and Figure 4B, white bars). The LC3-II protein level, however, was significantly and persistently increased in the pellet fractions, particularly in P1 and P2 fractions during 1 to 15 days of recovery after TBI (Figure 4A, LC3-II and Figure 4B, black bars). Pro-LC3 was detected only in S3 fraction and its level seemed to be not obviously altered after TBI (Figure 4A, S3, pro-LC3). Only LC3-I, but not LC3-II, was detected in S3 fraction (Figure 4A), consistent with previous reports (Tanida *et al*, 2004).

LC3 Distribution in Brain Sections after Traumatic Brain Injury

To study autophagic protein cellular distribution, we performed confocal microscopy of LC3 (green) and propidium iodide (red) in brain sections from sham-operated control rats and rats subjected to TBI followed by 24 h of recovery. Microtubule-associated protein light chain 3 immunoreactivity (green) was located mainly in neurons of both neocortical and CA3 areas (Figures 5A and 5C, arrows), as well as CA1 and DG regions (data not shown). The pattern of LC3 immunoreactivity was not obviously changed at the neocortical injury sites after TBI (Figures 5B and 5D, arrows). A fraction of propidium iodide-stained shrunken neurons in the neocortical and CA3 regions was not labeled by LC3 antibody in the post-TBI brain sections, because these neurons were damaged by TBI (Figures 5B and 5D, arrowheads). The neocortical and CA3 regions are major TBI foci in the fluid percussion injury model used in this study (Dietrich *et al*, 1996).

Discussion

This study shows that the autophagy pathway is markedly changed in vulnerable brain regions after TBI. Under EM, both APs and ALs accumulate markedly in neurons after TBI. Western blot analysis consistently clearly shows upregulation in two key autophagic markers, ATG12-ATG5 and LC3-II, in pre-AP- and AP-containing subcellular fractions during the post-TBI phase. Microtubule-associated protein light chain 3 immunoreactivity is located mainly in living neurons under confocal microscopy. The ultrastructural and biochemical results clearly show that the autophagy pathway is significantly activated in neurons after TBI. The autophagy pathway is the chief route for bulk degradation of damaged cell membranes, neuronal processes, and organelles after TBI. Therefore, activation of the autophagy pathway may play a key role in removing damaged cellular components after TBI.

Ultrastructural Features of Autophagy after Traumatic Brain Injury

All these ultrastructural features of autophagy are clearly observed by transmission EM in TBI neurons (see Figures 1 and 2). The ultrastructural hallmarks for induction of autophagy are the manifestation of (i) double-membraned cistern structures (see Figures 1 and 2); (ii) APs containing cytoplasmic materials or aberrant organelles (APs, see Figures 1 and 2); and (iii)

ALs that contain partially digested heterogeneous dense (dark) materials at an early stage and ultimately digested homogeneous dense material (ALs, see Figures 1 and 2). These results provide solid ultrastructural evidence showing that the autophagy pathway is activated after TBI.

Biochemical Changes in Autophagy after Traumatic Brain Injury

Biochemical hallmarks of autophagy initiation are the formation of two conjugates: (i) ATG12-ATG5 and (ii) LC3-II. ATG12-ATG5 is required for transformation from cup-shaped double-membraned cisterns to APs. Immediately before or after AP formation is completed, ATG12-ATG5 detaches from the membrane and is then recycled by ATG4 protease for the next round of AP formation (Mizushima *et al*, 2001). It remains unclear whether ATG12-ATG5 is also degraded during this process. This study shows that the ATG5 antibody predominantly labels the ATG12-ATG5 conjugated form (~53 kDa) mainly in S3 and P3 fractions but to a much lesser degree in P1 and P2 fractions (see Figure 3). The free or unconjugated ATG5 is barely detected in homogenate and cytosolic fractions (see Figure 3B, H and S3, arrowhead). The result is in line with previous reports showing that almost all ATG5 exists in the ATG12-ATG5 conjugated form (Mizushima *et al*, 2001). The predominant cytosolic pool of ATG12-ATG5 suggests that ATG12-ATG5 conjugate is ready to initiate AP formation in response to physiologic and pathologic changes. This is consistent with the fact that autophagy is a nonstop renewal process even under physiologic conditions. In addition, this study shows that ATG12-ATG5 in P3 fraction is significantly reduced at 4 h and is then drastically upregulated during the late periods of recovery after TBI. The changes in ATG12-ATG5 level in P3 fraction are likely because of its redistribution among P2, P3, and S3 fractions after TBI, because ATG12-ATG5 in homogenate is not significantly changed (see Figure 3). The late increases in ATG12-ATG5 in P3 fraction indicate that AP formation is upregulated during the late period of recovery after TBI. These results are consistent with the increases in APs and ALs observed by EM (see Figures 1 and 2).

Microtubule-associated protein light chain 3-II, as one of the mammalian homologues of ATG8-PE conjugate, is also recruited into double-membraned cisterns in an ATG12-ATG5-dependent manner (Mizushima *et al*, 2001). However, unlike ATG12-ATG5 conjugate that dissociates from the membrane immediately after AP formation, LC3-II conjugate remains on the AP membrane even after AP merges with lysosome (Kabeya *et al*, 2000). Hence, the LC3-II protein level has been used as a molecular marker to assess cellular AP numbers, and it has proved to be both more sensitive and specific than the less quantitative EM method (Koike *et al*, 2005). This study clearly shows that LC3-II is drastically and persistently upregulated in neurons from 1 day onward after TBI, thus providing solid quantitative evidence for dynamic upregulation of APs after TBI. The result is also complementary to the less quantitative EM observation of increases in APs after TBI (see Figures 1 and 2). In addition, upregulation of LC3-II is found mainly in P1 and P2 fractions but to a much lesser degree in the P3 fraction after TBI. This is consistent with the fact that LC3-II is located mainly in AP and also to a lesser degree in AL membranes (Kabeya *et al*, 2000; Tanida *et al*, 2004). In comparison with LC3-II, changes in ATG12-ATG5 conjugate occur mainly in S3 and P3 fractions after TBI. Taken together, these results support the fact that ATG12-ATG5 is associated with double-membrane cisterns (pre-APs) located in microsomal P3 fraction, whereas LC3-II in AP and AL membranes is distributed mainly into P1 and P2 fractions from brain tissues.

Confocal microscopic immunolabeling of LC3 in brain sections indicates that LC3 is mainly located in living neurons. However, the punctate LC3 immunostaining of APs seems not obvious after TBI. This may be due to a large non-AP LC3-I pool in neurons, as indicated by immunoblotting shown in Figure 4.

There are a few studies recently showing LC3 changes after brain hypoxia–ischemia (HI). Zhu *et al* (2005, 2006) reported that the LC3-II protein level was upregulated mainly in adult rather than neonatal brains after HI. Adhami *et al* (2006, 2007) found a reduction of LC3-I after HI but did not detect upregulation of LC3-II on immunoblot in mature HI mouse model. This study suggests that, relative to mild changes in LC3-II after HI in the previous reports, alterations in LC3-II after TBI appear more robust. During the revision of this paper, a study of autophagy after TBI in the ahead of print status by Lai *et al* (2007) also shows an increase in LC3-II in a mouse TBI model. The reason for the difference in the LC3-II level between TBI and HI is unknown, but it is probably because the pathophysiology incurred by TBI is far from identical to that of HI (Siesjo *et al*, 1995). Traumatic brain injury produces shear forces that primarily damage cell bodies and processes, whereas HI leads to metabolic failure (Bramlett and Dietrich, 2004; Zhu *et al*, 2006; Chu, 2006).

Significance of the Autophagy Pathway after Traumatic Brain Injury

On the basis of the fact that autophagy is a selfdefense mechanism for surviving environmental stress (Moore *et al*, 2006), activation of autophagy pathway is probably a neuroprotective response after TBI. To survive extreme environmental conditions or accidents such as TBI, neurons must make use of all available defense mechanisms to cope with accumulation of abnormal cellular structures after injury. Upregulation of the autophagy pathway, the chief machinery for bulk degradation of aberrant organelles, should be responsible for eliminating TBI-generated aberrant components to maintain neuronal homeostasis.

Although ATG gene knockout studies have clearly shown that the autophagy plays a key role in protecting neurons from protein aggregation-induced injury, in theory overactivation of autophagy might also carry potential risks. For example, overcrowded lysosomes might leak their hydrolases causing secondary cell injury. Autophagy has also been proposed to take part in cell death, the socalled “autophagic cell death”. Autophagic cell death has been suggested as a new mode of cell death distinct from both apoptosis and necrosis, and it is characterized by cytoplasmic accumulation of autophagic compartments (Swanson, 2006). Currently, it remains much controversial whether autophagic cell death is a tissue injury-accompanied epiphenomenon caused by an unsuccessful autophagic attempt to rescue dying cells or it is a programmed cell death response (Swanson, 2006). Several studies using chemical inhibitors of autophagy have led to inconclusive evidence, owing to the nonspecific properties of these inhibitors (Nixon, 2006; Klionsky, 2006). However, growing lines of evidence support the view that autophagy is essential for maintaining neuronal homeostasis: (i) deficiency in this pathway leads to neurodegeneration and human genetic diseases (Eskelinen, 2006; Nishino, 2006) and (ii) conditional knockout of key autophagic genes, ATG5 or ATG7, leads to accumulation of intracellular protein aggregates and neuronal death (Komatsu *et al*, 2006; Hara *et al*, 2006). Therefore, in most circumstances, induction of the autophagy pathway may be a cell protective response, and it is inadequate or defective autophagy, rather than excessive autophagy, that promotes neuronal death (Nixon, 2006). Future studies will determine whether and how manipulation of the autophagy pathway improves post-TBI recovery.

Acknowledgements

This work was supported by National Institutes of Health Grants NS040407, NS36810, and NS030291.

We thank Dr Brant Watson for proofreading this manuscript and Mrs Ofelia F Alonso for her assistance in producing the TBI model.

References

Adhami F, Liao G, Morozov YM, Schloemer A, Schmithorst VJ, Lorenz JN, Dunn RS, Vorhees CV, Wills-Karp M, Degen JL, Davis RJ, Mizushima N, Rakic P, Dardzinski BJ, Holland SK, Sharp FR, Kuan CY. Cerebral ischemia–hypoxia induces intravascular coagulation and autophagy. Am J Pathol 2006;169:566–83. [PubMed: 16877357]

Adhami F, Schloemer A, Kuan CY. The roles of autophagy in cerebral ischemia. Autophagy 2007;3:42–4. [PubMed: 17035724]

Bramlett HM, Dietrich WD. Pathophysiology of cerebral ischemia and brain trauma: similarities and differences. J Cereb Blood Flow Metab 2004;24:133–50. [PubMed: 14747740]

Brunk UT, Terman A. The mitochondrial–lysosomal axis theory of aging: accumulation of damaged mitochondria asa result of imperfect autophagocytosis. Eur J Biochem 2002;269:1996–2002. [PubMed: 11985575]

Chu CT. Autophagic stress in neuronal injury and disease. J Neuropathol Exp Neurol 2006;65:423–32. [PubMed: 16772866]

Ciechanover A. The ubiquitin proteolytic system: from a vague idea, through basic mechanisms, and onto human diseases and drug targeting. Neurology 2006;66(Suppl 1):S7–19. [PubMed: 16432150]

Dietrich WD, Alonso O, Halley M, Busto R. Delayed posttraumatic brain hyperthermia worsens outcome after fluid percussion brain injury: a light and electron microscopic study in rats. Neurosurgery 1996;38:533–41. [PubMed: 8837806]

Eskelinen EL. Roles of LAMP-1 and LAMP-2 in lysosome biogenesis and autophagy. Mol Aspects Med 2006;27:495–502. [PubMed: 16973206]

Hara T, Nakamura K, Matsui M, Yamamoto A, Nakahara Y, Suzuki-Migishima R, Yokoyama M, Mishima K, Saito I, Okano H, Mizushima N. Suppression of basal autophagy in neural cells causes neurodegenerative disease in mice. Nature 2006;441:885–9. [PubMed: 16625204]

Hu, BR. Co-translational protein folding and aggregation after brain ischemia. In: Lajtha, A., editor. Handbook of neurochemistry and molecular neurobiology. Vol. 3. Vol. 23. 2006. Chan, P., editor. Acute ischemic injury and repair in the nervous system. Berlin, Heidelberg, New York: Springer-Verlag; in press

Hu BR, Martone ME, Jones YZ, Liu CL. Protein aggregation after transient cerebral ischemia. J Neurosci 2000;20:3191–9. [PubMed: 10777783]

Hu BR, Park M, Martone ME, Fischer WH, Ellisman MH, Zivin JA. Assembly of proteins to postsynaptic densities after transient cerebral ischemia. J Neurosci 1998;18:625–33. [PubMed: 9425004]

Kabeya Y, Mizushima N, Yamamoto A, Oshitani-Okamoto S, Ohsumi Y, Yoshimori T. LC3, GABARAP and GATE16 localize to autophagosomal membrane depending on form-II formation. J Cell Sci 2004;117:2805–12. [PubMed: 15169837]

Kabeya Y, Mizushima N, Ueno T, Yamamoto A, Kirisako T, Noda T, Kominami E, Ohsumi Y, Yoshimori T. LC3, a mammalian homologue of yeast Apg8p, is localized in autophagosome membranes after processing. EMBO J 2000;19:5720–8. [PubMed: 11060023]

Kiselyov K, Jennigs JJ Jr, Rbaibi Y, Chu CT. Autophagy, mitochondria and cell death in lysosomal storage diseases. Autophagy 2007;3:259–62. [PubMed: 17329960]

Klionsky DJ. Autophagy. Curr Biol 2005;15:R282–3. [PubMed: 15854889]

Klionsky DJ. Neurodegeneration: good riddance to bad rubbish. Nature 2006;441:819–20. [PubMed: 16778876]

Koike M, Shibata M, Waguri S, Yoshimura K, Tanida I, Kominami E, Gotow T, Peters C, von Figura K, Mizushima N, Saftig P, Uchiyama Y. Participation of autophagy in storage of lysosomes in neurons from mouse models of neuronal ceroid-lipofuscinoses (Batten disease). Am J Pathol 2005;167:1713–28. [PubMed: 16314482]

Komatsu M, Waguri S, Chiba T, Murata S, Iwata J, Tanida I, Ueno T, Koike M, Uchiyama Y, Kominami E, Tanaka K. Loss of autophagy in the central nervous system causes neurodegeneration in mice. Nature 2006;441:880–4. [PubMed: 16625205]

Lai Y, Hickey RW, Chen Y, Bay H, Sullivan ML, Chu CT, Kochanek PM, Dixon CE, Jenkins LW, Graham SH, Watkins SC, Clark RS. Autophagy is increased after traumatic brain injury in mice and

is partially inhibited by the antioxidant gamma-glutamylcysteinyl ethyl ester. J Cereb Blood Flow Metab. 2007 September 5;e-pub ahead of print

Liu CL, Ge P, Zhang F, Hu BR. Co-translational protein aggregation after transient cerebral ischemia. Neuroscience 2005;134:1273–84. [PubMed: 16039801]

Martone ME, Jones YZ, Young SJ, Ellisman MH, Zivin JA, Hu BR. Modification of postsynaptic densities after transient cerebral ischemia: a quantitative and three-dimensional ultrastructural study. J Neurosci 1999;19:1988–97. [PubMed: 10066252]

Mizushima N, Yamamoto A, Hatano M, Kobayashi Y, Kabeya Y, Suzuki K, Tokuhisa T, Ohsumi Y, Yoshimori T. Dissection of autophagosome formation using Apg5-deficient mouse embryonic stem cells. J Cell Biol 2001;152:657–68. [PubMed: 11266458]

Moore MN, Allen JI, Somerfield PJ. Autophagy: role in surviving environmental stress. Mar Environ Res 2006;62:S420–5. [PubMed: 16709436]

Nishino I. Autophagic vacuolar myopathy. Semin Pediatr Neurol 2006;13:90–5. [PubMed: 17027858]

Nixon RA. Autophagy in neurodegenerative disease: friend, foe or turncoat? Trends Neurosci 2006;29:528–35. [PubMed: 16859759]

Ponten U, Ratcheson RA, Siesjo BK. Metabolic changes in the brains of mice frozen in liquid nitrogen. J Neurochem 1973;21:1211–6. [PubMed: 4761706]

Siesjo BK, Katsura K, Kristian T. The biochemical basis of cerebral ischemic damage. J Neurosurg Anesthesiol 1995;7:47–52. [PubMed: 7881240]

Swanson MS. Autophagy: eating for good health. J Immunol 2006;177:4945–51. [PubMed: 17015674]

Tanida I, Ueno T, Kominami E. LC3 conjugation system in mammalian autophagy. Int J Biochem Cell Biol 2004;36:2503–18. [PubMed: 15325588]

Yorimitsu T, Klionsky DJ. Autophagy: molecular machinery for self-eating. Cell Death Differ 2005;2 (Suppl):1542–52. [PubMed: 16247502]

Zhu C, Wang X, Xu F, Bahr BA, Shibata M, Uchiyama Y, Hagberg H, Blomgren K. The influence of age on apoptotic and other mechanisms of cell death after cerebral hypoxia–ischemia. Cell Death Differ 2005;12:162–76. [PubMed: 15592434]

Zhu C, Xu F, Wang X, Shibata M, Uchiyama Y, Blomgren K, Hagberg H. Different apoptotic mechanisms are activated in male and female brains after neonatal hypoxia–ischaemia. J Neurochem 2006;96:1016–27. [PubMed: 16412092]

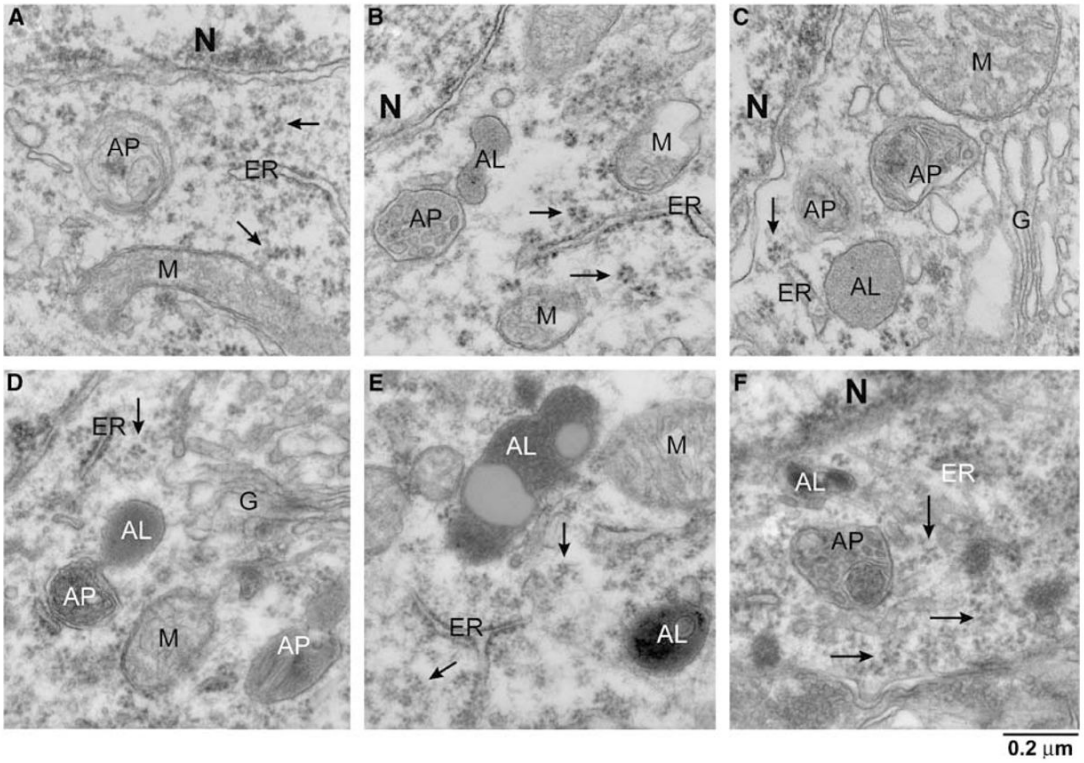

Figure 1.

Electron micrographs of neocortical neurons. (**A**) Sham-operated control; (**B**) 4 h; (**C**) 24h; (**D**) 3 days; (**E**) 5 days; and (**F**) 15 days after TBI. Brain sections were obtained from the neocortical area near the injury site (layers 3 to 5) and stained with the osmium–uranyl–lead method. Arrows point to polyribosomes. AP, autophagosome; AL, autolysosome; G, Golgi apparatus; ER, endoplasmic reticulum; M, mitochondrion; N, nucleus; Scale bars=0.2 μm.

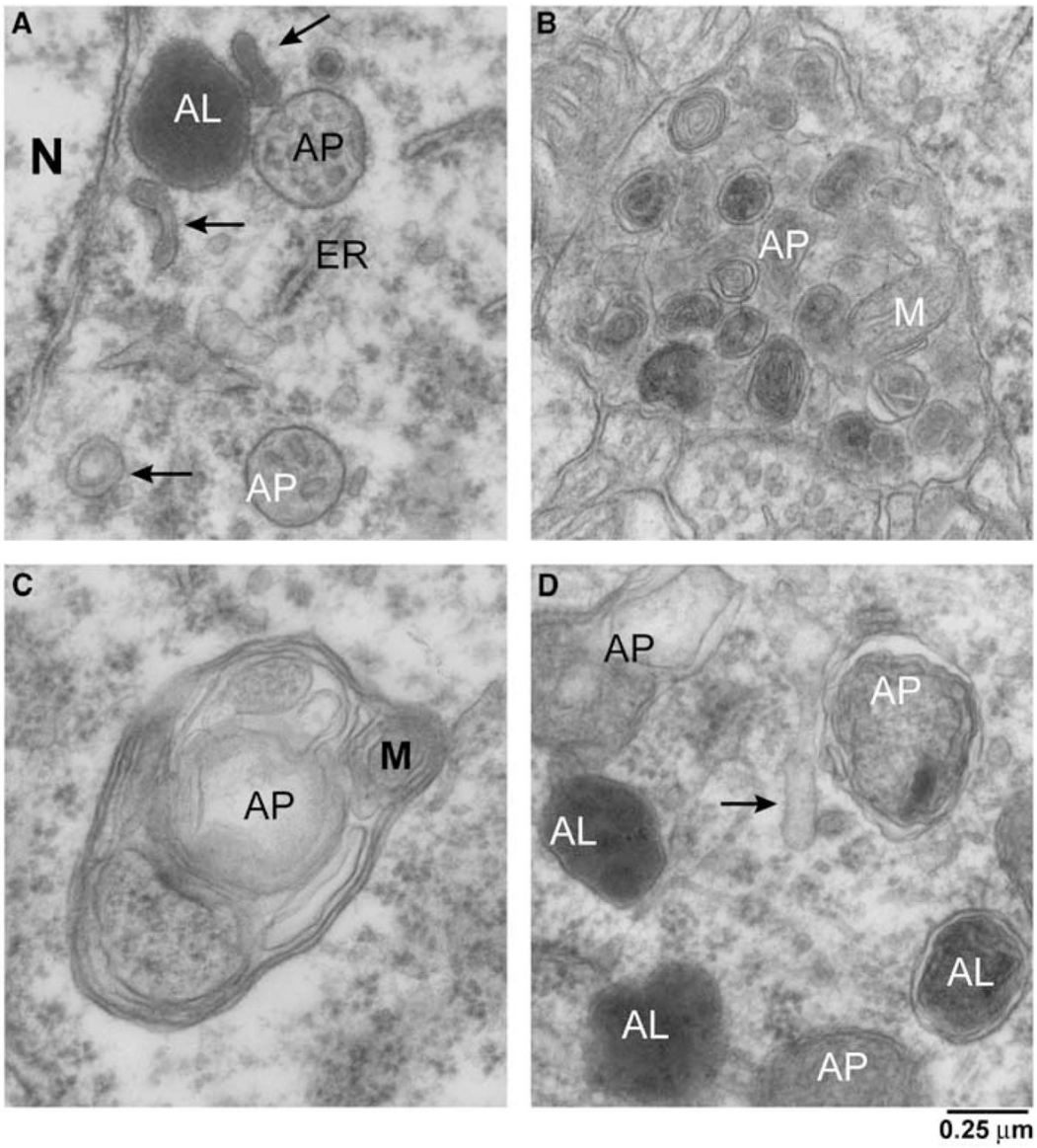

Figure 2.
Electron micrographs of autophagy-related vesicular compartments after TBI. Brain sections were obtained from the neocortical area near the injury site at 24 h after TBI (cortex layers 3 to 5). Several types of autophagic vacuoles are shown: (**A**) double-membraned cisterns or isolation membranes (arrows), autophagosome (AP), and autolysosome (AL); (**B**) autophagosomal clusters in the neuropil; (**C**) an AP containing a recognizable mitochondrion (M) in a dendritic trunk; and (**D**) autolysosomes (AL) with partially or completely digested organelles. Scale bar=0.25 μm.

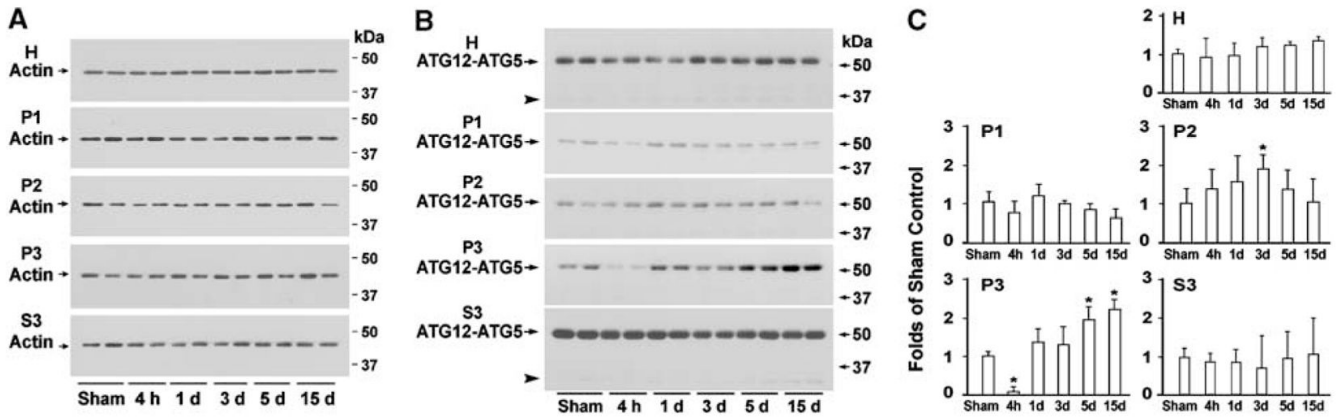

Figure 3.

(**A**) Immunoblots of *β*-actin. Brain samples were obtained from the neocortical injury regions of sham-operated control rats and rats subjected to TBI followed by 4 and 24 h, as well as 3, 5, and 15 days of recovery. Homogenate (H) and subcellular P1, P2, P3, and S3 fractions were immunoblotted with antibody to *β*-actin. Immunoblot membranes were then developed with Amersham ECL system. Two separate samples derived from two different rats in each experimental group are shown. (**B**) Immunoblots of ATG12-ATG5 conjugate and free unconjugated ATG5. The same brain samples as those in (**A**) were immunoblotted with ATG5 antibody that labels mainly ATG12-ATG5 conjugate (>50 kDa) and barely detects free ATG5. (**C**) Changes in conjugated ATG12- ATG5 protein level (~32 kDa, arrowhead). *β*-Actin as well as ATG12-ATG5 on immunoblots were evaluated with Kodak one-dimensional image software. The ATG12-ATG5 protein level was calculated by ATG12-ATG5/*β*-actin ratios using four different individual rat samples. Data are expressed as mean±s.d. (n=4). *P<0.05 between control and experimental conditions, one-way ANOVA followed by Dunnett's tests.

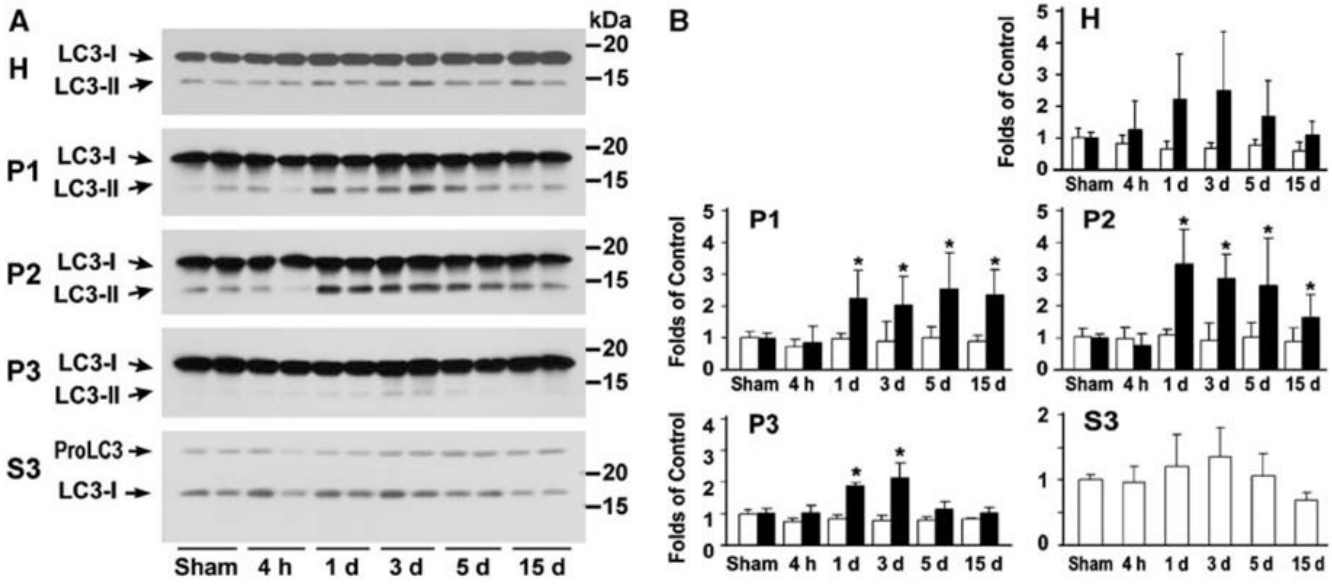

Figure 4.

(**A**) Immunoblots of pro-LC3, LC3-I, and LC3-II. Brain homogenate (H) and subcellular P1, P2, P3, and S3 fractions were prepared from the same sets of brains as those shown in Figure 3. Immunoblot membranes were labeled with LC3 antibody that recognized pro-LC3, as well as LC3-I (upper) and LC3-II (lower) on immunoblots, which were then developed with the ECL system. (**B**) Changes in LC3-I and LC3-II protein levels were evaluated and illustrated by LC3-I/*β*-actin (white bars) and LC3-II/*β*-actin ratios (black bars). Data are expressed as mean±s.d. (n=4). *P<0.05 between control and experimental conditions, one-way ANOVA followed by Dunnett's tests.

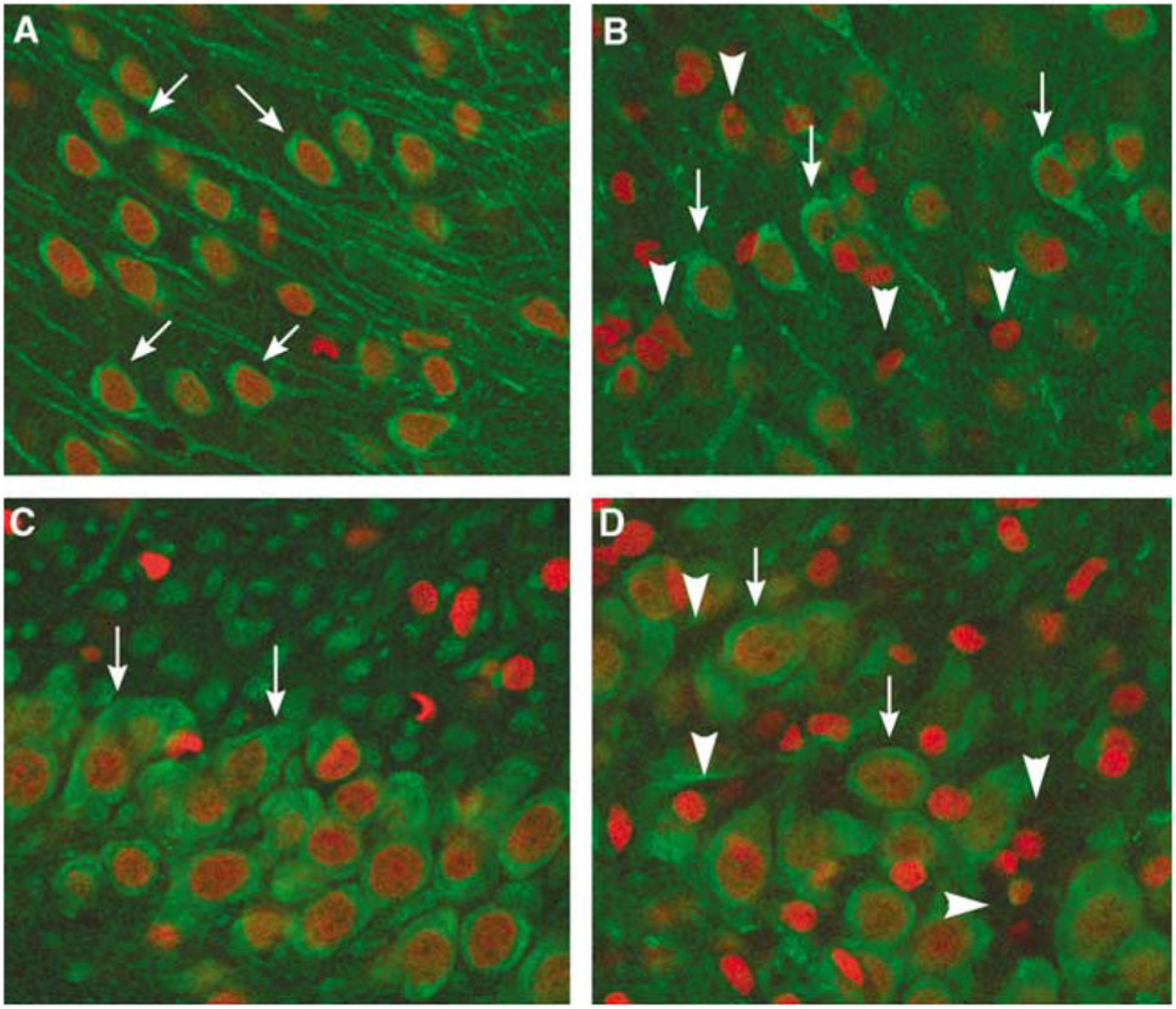

Figure 5.
Confocal microscopic images of LC-3 (green) and propidium iodide (PI, red). (**A**) Neocortical region (layers 3 to 4) of sham control; (**B**) neocortical region (layers 3 to 4) of TBI+24 h of recovery; (**C**) CA3 region (layers 3 to 4) of sham control; and (**D**) CA3 region (layers 3 to 4) of TBI+24 h of recovery. Brain sections were double labeled with LC3 antibody (green) and PI (red). Arrows denote LC3-positive neurons. Arrowheads point to PI-stained TBI-damaged shrunken neurons that were not labeled with LC3 antibody.